Effect of aminosilane nanoparticle coating on structural and magnetic properties and cell viability in human cancer cell lines

Israel Alejandro Flores Urquizo, Tomás Constantino Hernández García, Shadai Lugo Loredo, José Trinidad Elizalde Galindo Perla Elvia García Casillas Jazmín Cristina Stevens Barrón, Christian Chapa González**

I. A. Flores Urquizo
Instituto de Ingeniería y Tecnología (IIT), Universidad Autónoma de Ciudad Juárez (UACJ), Avenida del Charro 450, Partido Romero, 32584 Ciudad Juárez, Chihuahua, México

T. C. Hernández García
Facultad de Ciencias Químicas, Universidad Autónoma de Nuevo León (UANL), 66455, San Nicolás de los Garza, Nuevo León, México

S. Lugo Loredo
Facultad de Ciencias Químicas, Universidad Autónoma de Nuevo León (UANL), 66455, San Nicolás de los Garza, Nuevo León, México

J. T. Elizalde Galindo
Instituto de Ingeniería y Tecnología (IIT), Universidad Autónoma de Ciudad Juárez (UACJ), Avenida del Charro 450, Partido Romero, 32584 Ciudad Juárez, Chihuahua, México

P. E. García Casillas
Instituto de Ingeniería y Tecnología (IIT), Universidad Autónoma de Ciudad Juárez (UACJ), Avenida del Charro 450, Partido Romero, 32584 Ciudad Juárez, Chihuahua, México

J. C. Stevens Barrón
Instituto de Ciencias Biomédicas (ICB), Universidad Autónoma de Ciudad Juárez (UACJ), Estocolmo s/n, Zona Pronaf Condominio La Plata, 32310 Ciudad Juárez, Chihuahua, México

C. Chapa González
Instituto de Ingeniería y Tecnología (IIT), Universidad Autónoma de Ciudad Juárez (UACJ), Avenida del Charro 450, Partido Romero, 32584 Ciudad Juárez, Chihuahua, México

Keywords: nanomaterials, nanoparticles, magnetite, ferrite, superparamagnetic, cell viability, cancer

Magnetic nanoparticle interfaces have aroused great scientific research interest in the biomedical area since the interaction of cells or biomolecules with nanoparticles is determined by the surface properties. Currently, in medical applications there is a need to study cell interaction and growth, along with changes in structural or magnetic properties, attributed to nanoparticle coatings. In this work we evaluated the coercive field changes in $Ni_xFe_{3-x}O_4$ nanoparticles ($_x$ = 0.0, 0.2, 0.4, 0.6, 0.8 and 1.0) driven by partial or total substitution of Fe_{2+} content by Ni_{2+}, and by aminosilane coating. The nanoparticles were synthesized by the coprecipitation method. The inverse spinel structure is confirmed by X-ray diffraction results and Raman spectra. The aminosilane coating is confirmed by EDS and Fourier transform infrared spectroscopy. DLS confirmed a mean hydrodynamic size of 10 nm. Scanning electron microscopy micrographs of the uncoated and aminosilane-coated samples show that the particles have a hemispherical shape. The coating increases the coercive field. In addition, uncoated $Ni_{0.2}Fe_{2.8}O_4$ has the highest viability in both MCF7 and HeLa cell lines and aminosilane coating decreases cell viability. This work is a contribution to future applications of nanomedicine, such as hyperthermia and drug delivery.

1. Introduction

Nanoparticles exhibit interesting properties depending on their composition, morphology, size [1,2] and physicochemical properties of its surface. Interfaces and functional surfaces and their specific applications have driven the research and understanding of various interfacial processes that take place on nanoparticles in biological environments. In the past years, much attention has been paid to find the optimum properties for biomedical applications. [3–7] In the same way, some researchers have focused their attention on surface modification to improve the properties of the nanoparticles. [8–17]

One of the strategies that researchers have followed to modify the surface of nanoparticles and provide functionality has been to use coupling agents. Aminosilane is a coupling agent present in the nanomaterials used for biomedical applications. [18,19] Despite the influence on dispersion stability of the NPs, the aminosilane coating has a remarkable influence on the effectiveness of biomolecules immobilization.[20] Aminosilane compounds are widely described in the literature and their use has been validated for multiple biomedical applications to immobilize proteins, [21] enzymes, [16,22] antibodies, [23,24] nucleic acids,[25,26]

and drugs.[27] Although its extensive use as a coupling agent and its influence on the properties of nanomaterials have been reported for several nanomaterials, there are few attempts in the literature to study the effect of aminosilane on the properties of iron oxide nanomaterials, but they do not emphasize the influence of aminosilane on nanoparticle properties including cytotoxicity. The optimal level of these factors is very important to obtain high effectiveness and efficiency of these advanced materials for biomedical applications.

In particular, the development of magnetic nanoparticles is continuously progressing in terms of applications in biomedical field because one of its main features is their alternating magnetic field (AMF)-induced thermal effect or magnetic hyperthermia. [28–30] In clinical and experimental applications, heat generated by magnetic nanoparticles increases with the frequency (f) and the field strength (H) of AMF. [18,31,32] In addition to the field parameters, the magnetic nanoparticles dissipate heat from relaxation losses. [33,34] Among other properties such as anisotropy energy and rate of magnetic relaxation, the heating efficiency of magnetic nanoparticles depends on their superparamagnetic behavior, where coercivity, which must be near to zero, and the saturation magnetization (M_s) parameters play an important role in biomedical field. Therefore, it is needed to study the effect of aminosilane in structural and magnetic properties of the superparamagnetic nanoparticles.

Several research groups have established versatile methods to develop superparamagnetic magnetite nanoparticles (Fe_3O_4 NPs) which are considered one of the most promising materials for the induced thermal applications in biomedical area, due to their biocompatibility and adaptable surface modification [33,35,36]. Researchers have reported the varying in the M_s of Fe_3O_4 nanoparticles when changing the particle size, composition, and coatings. In the work presented by [32] the authors found that heat generation was strongly correlated with M_s (38.1 to 82.5 emu g^{-1}) and size (10 to 120 nm) of magnetite nanoparticles. In the same way, the findings described in [37] confirmed that the M_s increases when increasing particle size, from 54.7 emu g^{-1} (9.6 nm) to 84.7 emu g^{-1} (287 nm) regardless of the particle shape. Likewise, in [38] the M_s of carboxymethyl dextran and folic acid coated magnetite nanoparticles were found to be 35 emu g^{-1} and 30 emu g^{-1}, respectively, which were much less than the bare Fe_3O_4 nanoparticles, and to reach the temperature above 40 °C, with a frequency of 80 Hz, concentrations up to 55 mg/ml were necessary. In the work presented in [39], it is observed that the M_s of Fe_3O_4 nanoparticles (51.68 emu g^{-1}) were higher than the chitosan-coated Fe_3O_4 nanoparticles (49.96 emu g^{-1}), also, they observed that the temperature increases when the concentration of the suspensions increases (from 2 to 10 mg ml^{-1}).

Conversely, the temperature of coated nanoparticles was higher than the bare magnetite nanoparticles when increasing the intensity of the alternative magnetic field (from 167.6 to 335.2 Oe, f=265 Hz). The data presented indicate the importance of controlling M_s in biomedical applications.

Recently, there are reports of synthesis, doping, and cytotoxicity studies of nickel ferrite nanoparticles for biomedical applications. [40–43] The effect of the synthesis parameters on M_s of nickel ferrite nanoparticles is reported in literature. [44] [45] [46] [47] It has been shown that the coating of nickel ferrites has a greater influence on the M_s than the particle size. From the results obtained in [48] it was clear that coating $NiFe_2O_4$ nanoparticles with oleic acid decreased the M_s 5.4% while the variation in diameter from 5.4 to 16.2 nm varied the M_s by only 0.3%. However, further studies are needed that include Fe^{2+}/Ni^{2+} redistribution on nickel ferrite nanoparticles and the effect of the coating on magnetic properties and cell viability.

In the present study, we report the synthesis of the $Ni_xFe_{3-x}O_4$ (x = 0.0, 0.2, 0.4, 0.6, 0.8 and 1.0) nanoparticles by chemical coprecipitation and examine the influence of the aminosilane interface on the structural and magnetic properties of the nanomaterial. The purpose of this work is to study the effect caused by the surface modification of nanoparticles on properties such as magnetization. In addition, we study the cell viability of the nanoparticle preparations in MCF7 and HeLa cell lines to determine interactions of cells with surface modified nanoparticles.

2. Results and discussion

2.1 Obtained XRD patterns

The crystal structure and crystallite size of the samples were confirmed by X-ray diffraction (XRD) analysis. **Figure 1** a) shows the XRD patterns of Ni-substituted magnetite (x=0, 0.2, 0.4, 0.6, 0.8 and 1.0) in range 2θ between 15° and 90°. All the peaks in $Ni_xFe_{1-x}Fe_2O_4$ correspond to the characteristic inverse spinel (220), (311), (222), (400), (422), (511) and (400) crystal planes of magnetite and nickel ferrite standard XRD patterns, JCPDS 82-1533 and JCPDS 86-2267 respectively. Broadening of peaks in XRD patterns is increasing with the increment of Ni concentration in magnetite, indicating, continuous decrement of average crystallite size.

No peaks of impurities were observed in the XRD patterns, that indicates a good formation of the material by the selected technique. Moreover, there is no variation in the form of the structure maintaining the same inverse spinel cubic structure when varying the Fe^{2+} ions for Ni^{2+} ions. However, in sample x=0.8 is clearly seen that it has low crystallinity due to the poor differentiation of each diffraction peak. Since Ni^{2+} ions have smaller ionic radii (0.69 Å) than

Fe2+ ions (0.77 Å) at octahedral sites and x=0.8 is the highest substitution ratio of Fe^{2+} for Ni^{2+} ions in the sample series, all this leads to unit cell shrinkage causing crystal deformation. The crystallinity at x=1.0 is deduced from the observed line narrowing, the periodicity occurs because there are only Ni^{2+} ions in the octahedral sites.

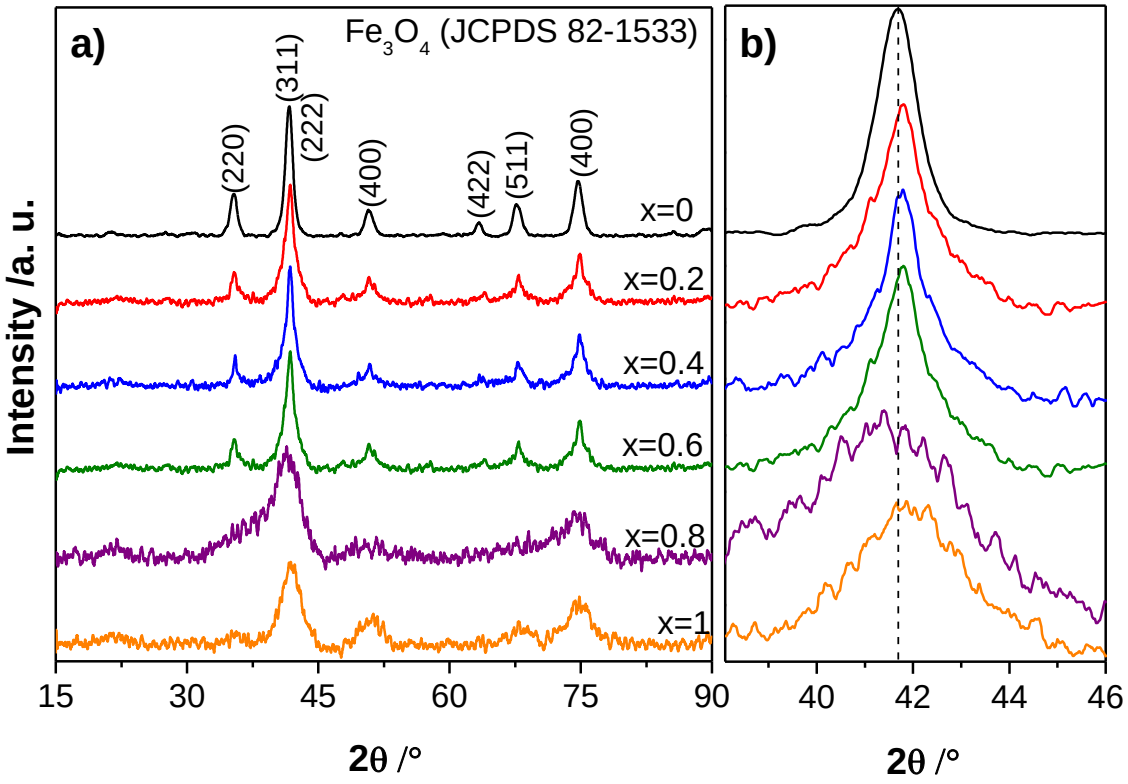

Figure 1 a) XRD patterns of Nickel substituted magnetite having the same eight peaks characteristic of a cubic spinel structure, b) magnified view of the (311) diffraction peak as a function of x

A quantitative evaluation of the crystallite sizes of the $Ni_xFe_{1-x}Fe_2O_4$ samples, was calculated by applying the Debye-Scherrer equation.

$$D = \frac{0.9\lambda}{\beta cos\theta} \quad (1)$$

Where λ is the wavelength of the X-ray radiation (Co, Kα=1.78Å), θ is the Bragg angle of the related peak, and β is the angular width of the peak at FWHM. [49] The diffraction peak (3 1 1) was selected for the calculation. The crystallite sizes of $Ni_xFe_{1-x}Fe_2O_4$ samples are in the range of 10 – 4 nm, for x=0 to x=1, respectively, demonstrating the efficacy of the proposed method to produce nano-size spinel $Ni_xFe_{1-x}Fe_2O_4$.

2.2 Study of size, morphology and elemental analysis of nanoparticles.

The average size for $Ni_xFe_{1-x}Fe_2O_4$ (X=0) obtained by TEM was 8.42 (**Figure 2a**). TEM analysis showed that the nanoparticles form clusters with sizes of about 20 nm. The morphology is uniform in hemispherical shape. In the same way, a coating layer is formed on the surface of

nanoparticles in the **Figure 2b** it is observed that the aminosilane coats a cluster of nanoparticles. There are reports in the literature describing the formation of such silica layers from TEOS[50] and silica-aminosilane[23] double coating. The DLS measurement (**Figure 3**) reports a size distribution around 10 nm,a polydispersity index of 0.324, and zeta potential -8.9 mV at pH 7.0. The size (hydrodynamic diameter) is larger than that obtained by TEM, which is attributed to the formation of the electric layer on the suspended charged particles. In the same sense, the nickel ferrite nanoparticles with AEPTMS have a size between 20 and 30 nm as observed in the SEM images (**Figure 4a**) and are the typical sizes obtained by the co-precipitation method as reported elsewhere.. [20,51–53] The size difference can be attributed to the aminosilane forming a layer and coating the nanoparticle clusters seen in the TEM. The presence of the coating in the samples subjected to the AEPTMS procedure was determined with the EDS spectrum (**Figure 4b**). In this spectrum the elements present in the sample whose energy kα of iron, nickel and silicon are observed at 6.40, 7.47 and 1.74 keV respectively are indicated. EDS spectrum has been employed elsewhere to analyze other silane-coated materials. [54,55]

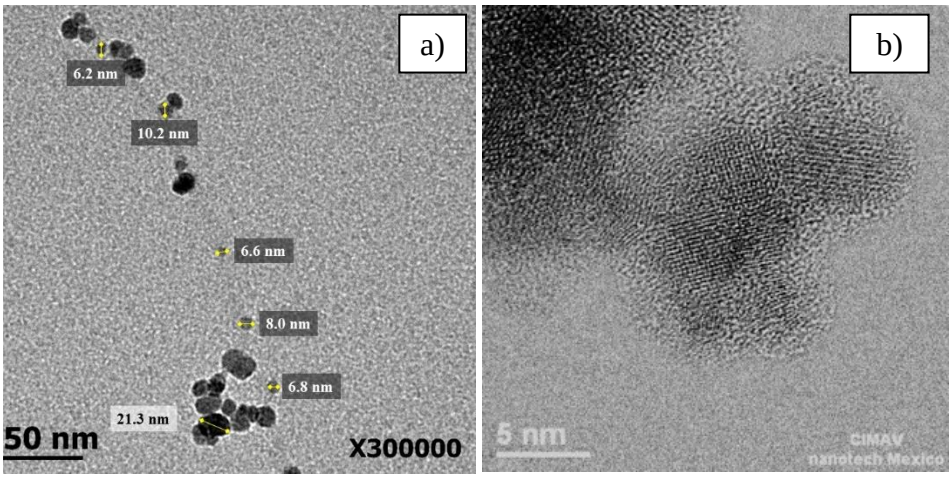

Figure 2 Bright field TEM image of sample a) $Ni_xFe_{1-x}Fe_2O_4$ ($_{X=0}$), showing semispherical nanoparticles with an average size of 8.42 nm, several clusters of nanoparticles with sizes around 20 nm are observed, b) aminosilane-coated $Ni_xFe_{1-x}Fe_2O_4$ ($_{X=0}$) nanoparticles, a layer of the aminosilane coating can be seen surrounding a cluster of nanoparticles

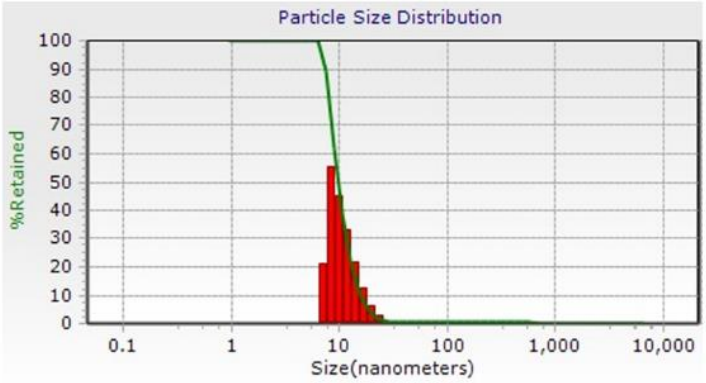

Figure 3 DLS measurement of $Ni_xFe_{1-x}Fe_2O_4$ ($X_{=0}$) with a polydispersity index of 0.324

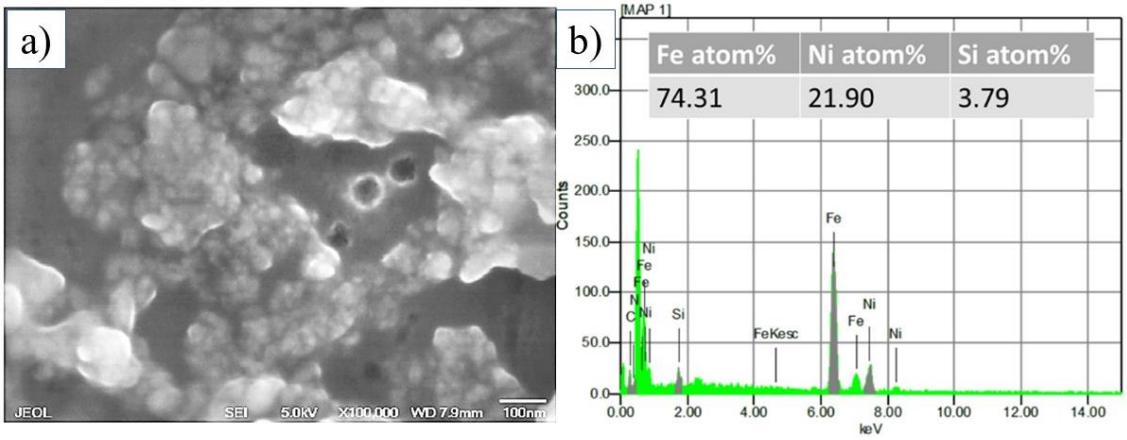

Figure 4 a) SEM image and b) EDS spectrum of AEPTMS-coated $Ni_xFe_{1-x}Fe_2O_4$ ($X_{=0}$) nanoparticles (x=1.0).

2.3 Infrared analysis of uncoated nanoparticles

The FTIR spectra of uncoated and coated material are displayed in **Figure 5**. In the IR spectra of uncoated particles (Figure 5a) a vibration band in around 634 cm^{-1} is attributed to vibrations of the metal-oxygen complexes in the octahedral sites [56], no other absorption bands shown due to the inorganic nature of the sample. The spectra of the aminosilane-coated nanoparticles are shown in Figure 5b. AEPTMS has a chemical architecture of one amino group at the end of two carbonate chains, which are joined by a secondary amine, and at the beginning of the chain are silicon and oxygen forming silica on the surface of the material. When comparing the obtained spectra with the functional groups of the coating, is observed that the vibrations bands of 3667 cm^{-1} and 812 cm^{-1} correspond to stretching and waging vibration of N-H bond, other vibration bands of 2980 cm^{-1} and 1402 cm^{-1} correspond to stretching and scissoring vibrations of C-H bond, additional stretching vibration modes like C-N, Si-O, Fe-O and O-H were found in 1240 cm^{-1}, 1085 cm^{-1}, 650 cm^{-1} and 2901 cm^{-1} respectively. The previous described bands are also found in APTES coating as reported in [51,52,55] due to AEPTMS and APTES have the same functional chemical groups.

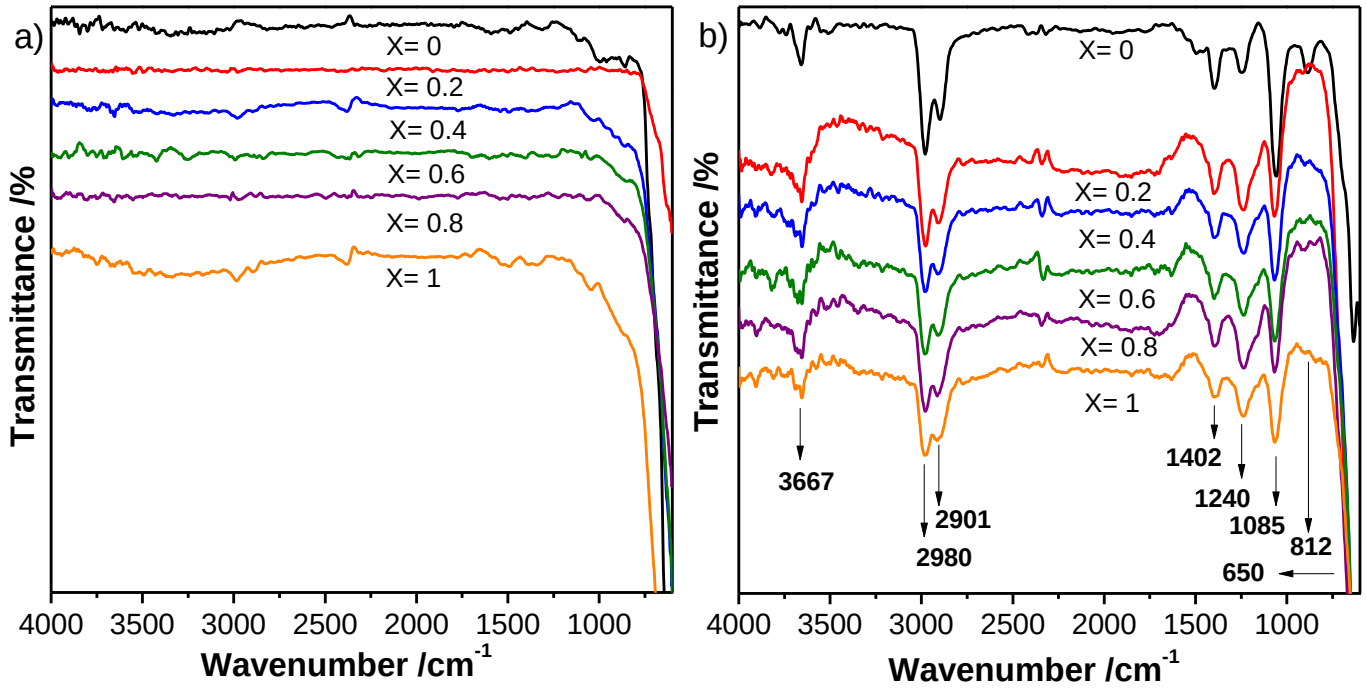

Figure 5 FTIR spectra of a) uncoated nanoparticles and b) aminosilane coated nanoparticles

2.4 Raman spectroscopy analysis

Raman spectroscopy is a crucial characterization technique to distinguish between different species of iron oxides, since they have different characteristic Raman modes, compared with X-ray diffraction that in some cases have very similar lattice attribute, which is difficult to observe the differences of each species. In **Figure 6**a the Raman spectra corresponding to the prepared phases of magnetite (x = 0) and nickel ferrites (x = 0.2, 0.4, 0.6, 0.8 and 1.0) are shown The main peaks corresponding to hematite phase (α-Fe_2O_3) were identified in the presented spectra in the form of well-defined sharp bands at 218 (A1g), 285 (E1g), 400 (E1g), 496 (A1g), 602 (E1g) cm^{-1} and a distant band at 1301 cm^{-1} roughly twice the frequency of a longitudinal optical phonon. [57] This occurs because magnetite has poor Raman scatter, particularly at low-power laser is required to keep the sample from undergoing laser irradiation induced phase transformation. [58] Also, hematite is one of the potential products of magnetite oxidation, this is given in Raman by the excessive exposure of the iron oxide sample to laser radiation. [59,60] In Figure 6b is displayed the deconvolution of the peak of the magnetite sample (x = 0) around 602 cm^{-1}, where bands corresponding to the magnetite (566 and 670 cm^{-1}) are observed. [61] In the samples with nickel content, a slight displacement is observed at lower frequencies. However, it also corresponds to the hematite phase. [57] The presence of a band at 1300 cm^{-1} in the nickel ferrites shows that there is Fe_2O_3, this changes as the substitution value increases until obtaining the nickel ferrite.

In Figure 6c, deconvoluted peaks and cumulative fit for the nickel ferrite are exposed. In

contrast to normal spinel ferrite structure, where M^{2+} cations are only in tetrahedral positions and Fe^{3+} exclusively in the octahedral sites, in the case of mixed spinel both sites are occupied by Ni^{2+} and by Fe^{3+} ions. A band observed at 201 cm^{-1} indicates the presence of possible traces of hematite in the nanoparticles and a band around 330 cm^{-1} that is assigned to a strong distortion of the ideal D3d symmetry for nickel ferrite nanoparticles. Two strong bands around 475 and 683 cm^{-1} are assigned to the tetrahedral (Fe^{3+} at A) and octahedral (Ni^{2+}, Fe^{3+} at B) sites respectively in the AB_2O_4 inverse spinel structure of ferrites. [62]

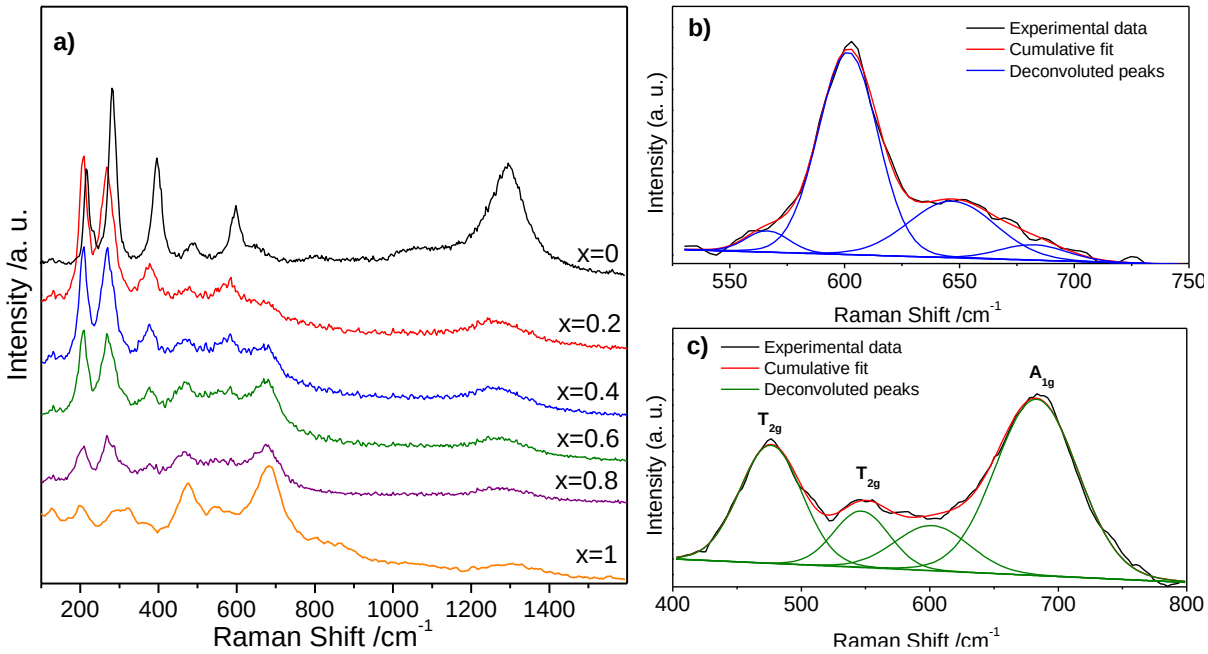

Figure 6 a) Raman spectra of elaborated $Ni_xFe_{1-x}Fe_2O_4$ samples (x = 0, 0.2, 0.4, 0.6, 0.8 and 1), (b) Deconvoluted peaks and cumulative fit for the sample without nickel in the range 530-750 cm^{-1} Raman shift, (c) Deconvoluted peaks and cumulative fit for the nickel ferrite in the range of 400-800 cm^{-1} of Raman shift

2.5 Magnetic properties of elaborated samples

The hysteresis loops of bare and AEPTMS-coated samples are shown in **Figure 7**. The curves show a hysteretic behavior without any irregular shape associated with mixtures of hard/soft spinel phases. The curves are consistent with the occurrence of a unique spinel cubic phase with a superparamagnetic behavior, these particles have the desire magnetic properties that make them attractive in the biomedical field. The figures show that the nickel content influences saturation magnetization and **Table 2** lists the obtained values. The M_s difference in ferrites can be explained based on the exchange interaction, where the Fe^{3+} ions are equally distributed between the octahedral and tetrahedral sites, and the Fe^{2+}/Ni^{2+} are in the octahedral sites in the inverse spinel crystal structure. The magnetic moments of Fe^{3+} ions are in an antiparallel sublattice between the tetrahedral and octahedral sites, and Ni^{2+}/Fe^{2+} ions occupy the octahedral

site, so the magnetic moment of these cations (2 μ_B/4 μ_B respectively) contribute to the magnetic properties of the inverse spinel structure. This results in a reduction of saturation magnetization as Ni^{2+} is substituting Fe^{2+} in octahedral site in the inverse spinel structure. For the concentration up to x = 0.8 in $Ni_xFe_{1-x}Fe_2O_4$, the typical trend in the decrement of magnetization is obtained despite cation inversion. However, as we approach x = 1, the particle size is small enough to get a cation inversion degree. The concentration of Ni, the low crystallinity observed in Figure 1 and the very fine particle size, are responsible for the low saturation magnetization $Ni_{0.8}Fe_{2.2}O_4$ as expected according to the trend. The coercive field of these samples also shows a decrease in their value when nickel was added. This phenomenon is correlated with the crystallite size according to Table 2, so when the size of the particles decreases, the coercivity also decrease.

The small reduction on M_s of AEPTMS coated nanoparticles, compared with bare nanoparticles is attributed to the presence of coating that affect the total mass of the sample (magnetic core mass + nonmagnetic shell mass). This effect is also reported in magnetic nanoparticles coated with APTES and silica. [51,53,54] According to Table 1, the AEPTMS reaches a slight increment of coercivity. This behavior is attributed to an alteration in the surface anisotropy of particles caused by the interparticle dipolar fields with the silica formed on the particle surface in AEPTMS coating.

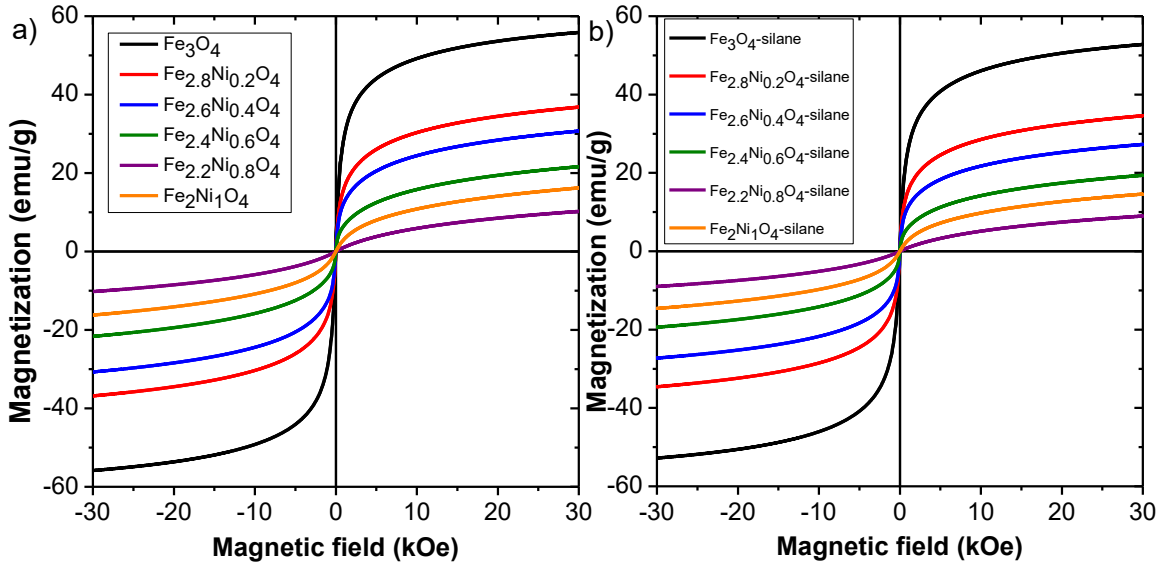

Figure 7 Hysteresis loops of a) uncoated and b) AEPTMS coated iron/nickel magnetic nanoparticles

Table 1 Magnetic properties of bare and AEPTMS coated $Ni_xFe_{1-x}Fe_2O_4$ samples

	Uncoated nanoparticles		AEPTMS coated nanoparticles		
Sample	Saturation magnetization [emu g^{-1}]	Coercive field [Oe]	Saturation magnetization [emu g^{-1}]	Coercive field [Oe]	Crystallite size [nm]
Fe_3O_4	55.84	29.32	52.78	35.17	10.39
$Ni_{0.2}Fe_{2.8}O_4$	36.81	12.09	34.61	12.80	8.71
$Ni_{0.4}Fe_{2.6}O_4$	30.71	11.22	27.27	18.67	9.56
$Ni_{0.6}Fe_{2.4}O_4$	21.64	8.26	19.41	10.95	5.70
$Ni_{0.8}Fe_{2.2}O_4$	10.21	1.37	9.01	4.50	2.81
$NiFe_2O_4$	16.21	4.77	14.59	6.04	3.86

2.6 Cell viability

Breast cancer cell line MCF-7 and cervical cancer cell line HeLa are widely applied research and development of biomedical engineering areas such as nanoparticle mediated drug release and hyperthermia. [63] Therefore, MCF-7 and HeLa cell line are appropriate for cell viability determination of nanomaterials designed for nanomedicine applications. The cell viability of MCF-7 and HeLa exposed to nickel ferrites $Ni_xFe_{3-x}O_4$ (x=0.2, 0.4, 0.6, 0.8 and 1.0) at a concentration of 50 μg ml^{-1} was evaluated by MTT assay after an exposure of 48 h (**Figure** 8). The elaborated MTT assays indicate that the dosage of nickel doped nanoparticles was elevated, this affects the cell viability of the cell lines, diminishing the mitochondrial reduction to transform MTT to formazan indicating cell death. According to the ISO 10993-5 the cell viability in all samples except bare $Fe_{2.8}Ni_{0.2}O_4$ were below 70% so the concentration of 50 μg ml^{-1} is considered cytotoxic, a cell viability study modifying the Ni doped ferrites concentration in the same cell lines would help to obtain a less cytotoxic dosage. In general, cell viability was lower in the nanomaterials with the aminosilane coating. This can be attributed to the fact that the coating decreases the agglomeration of the nanoparticles and therefore can easily penetrate inside the cells causing cell death. In addition, it has been shown that the silica on the surface can be eroded by the ingredients in DMEM [64], so cells can be exposed to the materials in the core and also to coating residues that can be harmful.

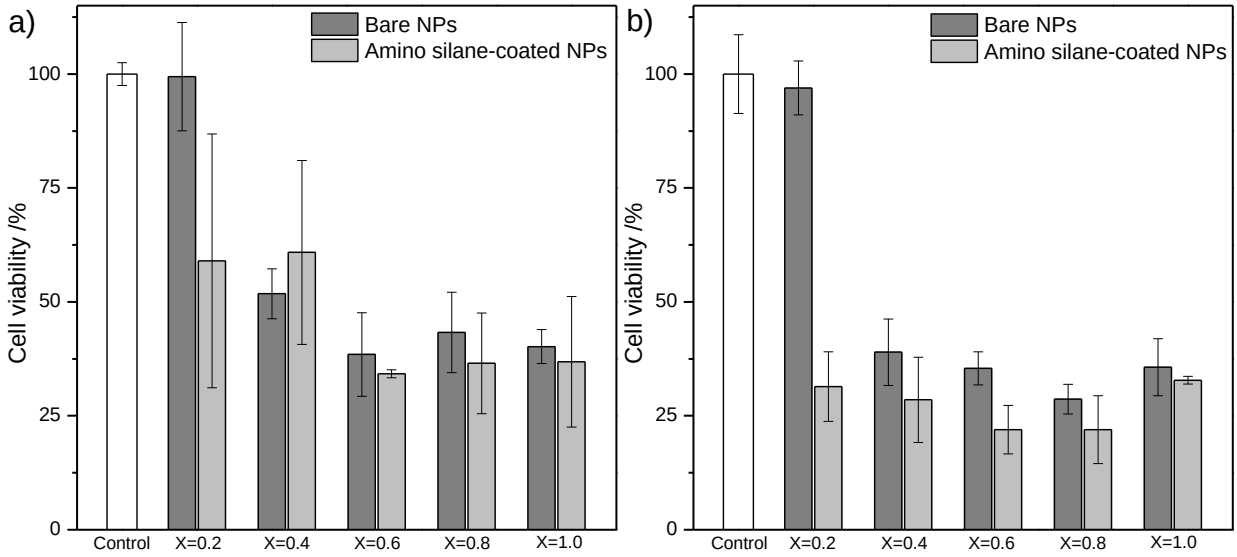

Figure 8 Cell viability of a) MCF-7 cells and b) HeLa cells using MTT assay versus stoichiometric ratio of Ni^{2+} in bare and aminosilane-coated $Ni_xFe_{3-x}O_4$ nanoparticles. Error bars = standard error on the mean. The cells were incubated with the indicated nickel ferrite for 48 h (white bar) in a medium with bare nanoparticles and (grey bar) in a medium with aminosilane-coated nickel ferrite nanoparticles

3. Conclusion

A facile and convenient coprecipitation procedure was adopted for the synthesis, and further aminosilane-surface modification, of ferrite nanoparticles with different concentrations of nickel. The obtained materials showed only a single phase in the XRD patterns. The FTIR spectra support the evidence of coating in the aminosilane-treated ferrites. Several bands appeared in the IR spectra after the treatment of the particles with aminosilane among them, the bands attached to the N-H and Si-O bonds. Likewise, both magnetite and nickel ferrite are inverse spinels, having Fe^{3+} ions only at the tetrahedral sites. Evidently, crystal field perturbations have a significant effect on the Raman spectra that evidenced cation exchange in the different compositions. The obtained nanoparticles possess a spherical morphology and the particle size decreased when increasing the content of nickel. All the samples exhibit superparamagnetic behavior, and the saturation magnetization varies by substituting the Fe^{2+} with the Ni^{2+} ion in the synthesis reaction. Coating nanoparticles with aminosilane decreased the M_s 10%. Overall, the cell viability of MCF-7 breast cancer cells and cervical cancer cells decreased with the coating so these materials can be employed in targeted therapies. In addition, there is a need to study the erosion of the aminosilane coating to evaluate its effect on cell viability in future research. The tailoring features of size, composition and saturation magnetization enable the ferrite nanoparticles to be used as advanced materials in alternating magnetic field (AMF)-induced thermal effect in biomedical area.

4. Experimental Section

Materials and experimental method: **Iron(III) chloride hexahydrate ($FeCl_3 \cdot 6H_2O$), iron(II) sulfate heptahydrate ($FeSO_4 \cdot 7H_2O$), nickel(II) sulfate hexahydrate ($NiSO_4 \cdot 6H_2O$), ammonium hydroxide (NH_4OH) 30% solution, and [3-(2-Aminoethylamino) propyl] trimethoxysilane (AEPTMS) were purchased from Sigma Aldrich and used without further purification.**

Magnetite Fe_3O_4 nanoparticles were synthesized by alkaline coprecipitation of two equivalents of iron(III) chloride hexahydrate and one equivalent of iron(II) sulfate heptahydrate in ammonium hydroxide solution with stirring. To obtain nickel ferrites, $Ni_xFe_{3-x}O_4$ (x = 0.0, 0.2, 0.4, 0.6, 0.8 and 1.0), the volume and concentration of the ferric chloride solution remained the same in all reactions (100 mL, 0.10 M), and nickel(II) sulfate heptahydrate solution was replaced instead of iron(II) solution adjusting the stoichiometry (**Table 2**).

Samples were modified using a two-step method to obtain aminosilane-coated nanoparticles reported elsewhere. [65] The coating process was realized dispersing (0.10 g) of each ferrite sample in ethanol (150 ml)applying ultrasonic stirring. Then a solution with [3-(2-Aminoethylamino) propyl] trimethoxysilane was added, the detailed process is reported elsewhere. [51,65] After this step, all elaborated samples with coating and without coating were stored to characterize them.

Table 2 Concentrations of solutions used to obtain the nickel ferrites

Nickel ferrite $Ni_xFe_{3-x}O_4$	Ni^{2+}	Ni^{2+} solution 50 ml [M]	Fe^{2+}	Fe^{2+} solution 50 ml [M]	Fe^{3+} solution 100 ml [M]
$Ni_{0.2}Fe_{2.8}O_4$	0.2	0.01	0.8	0.04	0.10
$Ni_{0.4}Fe_{2.6}O_4$	0.4	0.02	0.6	0.03	
$Ni_{0.6}Fe_{2.4}O_4$	0.6	0.03	0.4	0.02	
$Ni_{0.8}Fe_{2.2}O_4$	0.8	0.04	0.2	0.01	

Characterization methods

Powder X-ray diffraction (XRD). Analysis of the synthetized powders was achieved using a Siemens D500 diffraction system with a cobalt Kα radiation source (λ=1.78897Å). The scan was realized over the 2θ range of 15° to 90°. PANalytical X'pert HighScore software was

employed to analyze the obtained data.

Scanning Electron Microscope (SEM). The powder samples were prepared on a carbon adhesive tape to support the sample inside the microscope. The micrographs were taken using a JEOL6010 PLUS/LA, TEM was also used to elucidate the size of the nanoparticles using the 'ImageJ' software.

Energy-dispersive X-ray spectroscopy (EDS). Elemental composition analysis was acquired by a JEOL6010 PLUS/LA, the measures were taken in three different zones of each sample.

Dynamic Light Scattering (DLS). This technique was used to measure the hydrodynamic size of elaborated Fe_3O_4 nanoparticles, nanoparticles were dispersed in (1%) Triton 100X solution. The measure was repeated three times using a MICROTRAC (Nanotrac Wave) particle size analyzer.

Fourier-Transform Infrared Spectroscopy (FTIR). Infrared spectroscopy was employed to obtain the IR spectra of the samples coated with aminosilane, the spectrum of each sample was recorded from 4000 cm^{-1} to 600 cm^{-1} to obtain information about the organic coating applied. The equipment used was a Nicolet 6700 spectrometer of Thermo Fisher Scientific.

Vibrating Sample Magnetometry (VSM). Magnetic properties of the elaborated nanoparticles were measured using a Versalab Crio Free vibrating sample magnetometer of Quantum Design. The hysteresis loops were measured at 300 K using an applied field up to 3 Tesla. The saturation magnetization of the samples was calculated in terms of the hysteresis loops.

Raman spectra were taken by placing the sample (0.1 g) on a microscope slide. The sample was spread to obtain a uniform film. The samples were excited with a 532 nm laser beam in a WITec Raman microscopy.

To examine the cell viability of the nanoparticles, an *in vitro* methyl thiazolyl tetrazolium (MTT) assay was performed using MCF-7 and HeLa cell lines. The cells were seeded in an DMEM culture media containing 5% fetal bovine serum with (200 U mL^{-1}) penicillin-streptomycin. MCF-7 and HeLa cells were seeded into a separated 96-well cell culture plate at 10 000 per well and then incubated for 24 h at 37 °C under 5% CO_2. Then, nanoparticles dispersed in PBS were added to each well to give final particle concentration (50 µg ml^{-1}). The cells were then incubated for 48 h at 37 °C under 5% CO_2. At the end of the incubation time, nanoparticles containing media was removed, wells were washed using PBS to remove the non-uptaken particles and 90 µl of fresh medium was added. Then filter-sterilized MTT reagent in PBS (5 mg mL^{-1}) of was added to each well (100 µl), and the plates were incubated at 37 °C under 5% CO_2 for further 4 h. After incubation, the culture medium was discarded and (100 µl) DMSO were added to each well to dissolve the formazan crystals. Absorption values of the

dissolved formazan crystals in each well were measured at 570 nm using a microplate reader. Cell viability was defined as the percentage ratio of the absorbance of the treated cells to the untreated control. All the samples were prepared in triplicate.

Conflict of Interest

The authors have no conflicts of interest to declare

Acknowledgements

We would like to thank the members of the Nanomedicina-UACJ research group for the feedback received during the research.

Data Availability Statement

The data that support the findings of this study are available from the corresponding author upon reasonable request.

Received: ((will be filled in by the editorial staff))

Revised: ((will be filled in by the editorial staff))

Published online: ((will be filled in by the editorial staff))

References

1 A. L. Tiano, G. C. Papaefthymiou, C. S. Lewis, J. Han, C. Zhang, Q. Li, C. Shi, A. M. M. Abeykoon, S. J. L. Billinge, E. Stach, J. Thomas, K. Guerrero, P. Munayco, J. Munayco, R. B. Scorzelli, P. Burnham, A. J. Viescas, S. S. Wong, *Chemistry of Materials* **2015**, *27*, 3572.

2 F. J. Carrillo-Pesqueira, R. C. Carrillo-Torres, M. E. Álvarez-Ramos, J. Hernández-Paredes, *Microscopy and Microanalysis* **2018**, *24*, 1098.

3 R. Esquivel, J. Juárez, M. Almada, J. Ibarra, M. A. Valdez, *International Journal of Polymer Science* **2015**, *2015*, 1.

4 S. Correa-Espinoza, C. A. Rodríguez-González, S. A. Martel-Estrada, J. F. Hernández-Paz, I. Olivas-Armendáriz, *Journal of Non - Oxide Glass* **2018**, *10*, 1.

5 K. Maldonado-Lara, G. Luna-Bárcenas, E. Luna-Hernández, F. Padilla-Vaca, E. Hernández-Sánchez, R. Betancourt-Galindo, J. R. Menchaca-Arredondo, B. L. España-Sánchez, *Revista Mexicana de Ingeniería Biomédica* **2017**, *38*, 306.

6 J. Roacho-Perez, H. Gallardo-Blanco, M. Sanchez-Dominguez, P. Garcia-Casillas, C. Chapa-Gonzalez, C. Sanchez-Dominguez, *Molecular Medicine Reports* **2017**, *17*, 1413.

7 T. Ruthradevi, J. Akbar, G. Suresh Kumar, A. Thamizhavel, G. A. Kumar, R. K. Vatsa, G. C. Dannangoda, K. S. Martirosyan, E. K. Girija, *Journal of Alloys and Compounds* **2017**, *695*, 3211.

8 A. K. Gupta, M. Gupta, *Biomaterials* **2005**, *26*, 3995.

9 N. D. Thorat, V. M. Khot, A. B. Salunkhe, R. S. Ningthoujam, S. H. Pawar, *Colloids and Surfaces B: Biointerfaces* **2013**, *104*, 40.
10 A. Tomitaka, T. Koshi, S. Hatsugai, T. Yamada, Y. Takemura, *Journal of Magnetism and Magnetic Materials* **2011**, *323*, 1398.
11 L. Mao, X. Liu, M. Liu, L. Huang, D. Xu, R. Jiang, Q. Huang, Y. Wen, X. Zhang, Y. Wei, *Applied Surface Science* **2017**, *419*, 188.
12 S. Mallakpour, R. Sadeghzadeh, *Polymers for Advanced Technologies* **2017**, *28*, 1719.
13 W. Wu, Q. He, C. Jiang, *Nanoscale Research Letters* **2008**, *3*, 397.
14 C. Chapa Gonzalez, J. A. Roacho Pérez, C. A. Martínez Pérez, I. Olivas Armendáriz, F. Jimenez Vega, K. Y. Castrejon Parga, P. E. Garcia Casillas, *Journal of Alloys and Compounds* **2015**, *615*, S655.
15 A. Liberman, N. Mendez, W. C. Trogler, A. C. Kummel, *Surface Science Reports* **2014**, *69*, 132.
16 F. Šulek, M. Drofenik, M. Habulin, Ž. Knez, *Journal of Magnetism and Magnetic Materials* **2010**, *322*, 179.
17 C. He, Y. Hu, L. Yin, C. Tang, C. Yin, *Biomaterials* **2010**, *31*, 3657.
18 K. Maier-Hauff, R. Rothe, R. Scholz, U. Gneveckow, P. Wust, B. Thiesen, A. Feussner, A. von Deimling, N. Waldoefner, R. Felix, A. Jordan, *Journal of Neuro-Oncology* **2007**, *81*, 53.
19 S. V Spirou, M. Basini, A. Lascialfari, C. Sangregorio, C. Innocenti, *Nanomaterials (Basel)* **2018**, *8*.
20 E. Villegas-Serralta, O. Zavala, I. A. Flores-Urquizo, P. E. García-Casillas, C. Chapa González, *Journal of Nanomaterials* **2018**, *2018*, 1.
21 X. Liu, J. Xing, Y. Guan, G. Shan, H. Liu, *Colloids and Surfaces A: Physicochemical and Engineering Aspects* **2004**, *238*, 127.
22 L. Križnik, K. Vasić, Ž. Knez, M. Leitgeb, *Journal of Cleaner Production* **2018**, *179*, 225.
23 C. Chapa Gonzalez, C. A. Martínez Pérez, A. Martínez Martínez, I. Olivas Armendáriz, O. Zavala Tapia, A. Martel-Estrada, P. E. García-Casillas, *Journal of Nanomaterials* **2014**, *2014*, 978284.
24 E. Villegas-Serralta, O. Zavala, I. A. Flores-Urquizo, P. E. García-Casillas, C. Chapa González, *Journal of Nanomaterials* **2018**, 7571613.
25 T. Tanaka, R. Sakai, R. Kobayashi, K. Hatakeyama, T. Matsunaga, *Langmuir* **2009**, *25*, 2956.
26 W. Sheng, W. Wei, J. Li, X. Qi, G. Zuo, Q. Chen, X. Pan, W. Dong, *Applied Surface Science* **2016**, *387*, 1116.
27 R. P. Dhavale, P. P. Waifalkar, A. Sharma, R. P. Dhavale, S. C. Sahoo, P. Kollu, A. D. Chougale, D. R. T. Zahn, G. Salvan, P. S. Patil, P. B. Patil, *Journal of Colloid and Interface Science* **2018**, *529*, 415.
28 M. Suto, H. Kosukegawa, K. Maruta, M. Ohta, K. Tohji, B. Jeyadevan, *Journal of Magnetism and Magnetic Materials* **2009**, *321*, 3483.
29 M. Dan, Y. Bae, T. A. Pittman, R. A. Yokel, *Pharm Res* **2015**, *32*, 1615.
30 A. Jordan, P. Wust, H. Fähling, W. John, A. Hinz, R. Felix, *Int J Hyperthermia* **2009.**, *9*, 51.
31 B. Thiesen, A. Jordan, *International Journal of Hyperthermia* **2008**, *24*, 467.
32 J. Motoyama, T. Hakata, R. Kato, N. Yamashita, T. Morino, T. Kobayashi, H. Honda, *Biomagn Res Technol* **2008**, *6*, 4.
33 A. Sohail, Z. Ahmad, O. A. Bég, S. Arshad, L. Sherin, *Bulletin du Cancer* **2017**, *104*, 452.
34 I. M. Obaidat, B. Issa, Y. Haik, *Nanomaterials (Basel)* **2015**, *5*, 63.
35 D. Ling, T. Hyeon, *Small* **2013**, *9*, 1450.

36 R. V. Mehta, *Materials Science and Engineering: C* **2017**, *79*, 901.
37 Q. Li, C. W. Kartikowati, S. Horie, T. Ogi, T. Iwaki, K. Okuyama, *Scientific Reports* **2017**, *7*, 9894.
38 Q. L. Jiang, S. W. Zheng, R. Y. Hong, S. M. Deng, L. Guo, R. L. Hu, B. Gao, M. Huang, L. F. Cheng, G. H. Liu, Y. Q. Wang, *Applied Surface Science* **2014**, *307*, 224.
39 P. B. Shete, R. M. Patil, N. D. Thorat, A. Prasad, R. S. Ningthoujam, S. J. Ghosh, S. H. Pawar, *Applied Surface Science* **2014**, *288*, 149.
40 I. Sharifi, H. Shokrollahi, S. Amiri, *Journal of Magnetism and Magnetic Materials* **2012**, *324*, 903.
41 S. Khan, A. A. Ansari, A. Malik, A. A. Chaudhary, J. B. Syed, A. A. Khan, *Journal of Trace Elements in Medicine and Biology* **2019**, *52*, 12.
42 F. Ibraheem, M. H. Aziz, M. Fatima, F. Shaheen, S. M. Ali, Q. Huang, *Materials Letters* **2019**, *234*, 129.
43 M. Amiri, A. Pardakhti, M. Ahmadi-Zeidabadi, A. Akbari, M. Salavati-Niasari, *Colloids and Surfaces B: Biointerfaces* **2018**, *172*, 244.
44 H. Ghayour, M. Abdellahi, N. Ozada, S. Jabbrzare, A. Khandan, *Journal of Physics and Chemistry of Solids* **2017**, *111*, 464.
45 X. Liu, W.-L. Gao, *Materials and Manufacturing Processes* **2012**, *27*, 905.
46 S. Asiri, M. Sertkol, H. Güngüneş, Md. Amir, A. Manikandan, İ. Ercan, A. Baykal, *Journal of Inorganic and Organometallic Polymers and Materials* **2018**, *28*, 1587.
47 O. Karaagac, S. Atmaca, H. Kockar, *Journal of Superconductivity and Novel Magnetism* **2017**, *30*, 2359.
48 R. Kurosawa, T. Suzuki, T. Nakayama, H. Suematsu, K. Niihara, *Japanese Journal of Applied Physics* **2011**, *50*, 01BE11.
49 G. Rana, U. C. Johri, *Journal of Alloys and Compounds* **2013**, *577*, 376.
50 Jaeyun K., Hoe Suk K., Nohyun L., Taeho K., Hyoungsu K. ,Taekyung Y., In Chan S. P., Woo Kyung M.., Taeghwan H. *Angewandte Chemie* **2008,** 47(44).
51 M. Yamaura, R. L. Camilo, L. C. Sampaio, M. A. Macêdo, M. Nakamura, H. E. Toma, *Journal of Magnetism and Magnetic Materials* **2004**, *279*, 210.
52 K. Can, M. Ozmen, M. Ersoz, *Colloids and Surfaces B: Biointerfaces* **2009**, *71*, 154.
53 S. Sundar, R. Mariappan, S. Piraman, *Powder Technology* **2014**, *266*, 321.
54 J. Zou, Y. Xu, B. Hou, D. Wu, Y. Sun, *Powder Technology* **2008**, *183*, 122.
55 T. Mu, J. Zhao, Y. Guan, J. Tian, M. Yang, C. Guo, J. Xing, *Biotechnology Letters* **2017**, *39*, 865.
56 M. A. Haija, A. F. S. Abu-Hani, N. Hamdan, S. Stephen, A. I. Ayesh, *Journal of Alloys and Compounds* **2017**, *690*, 461.
57 I. Chourpa, L. Douziech-Eyrolles, L. Ngaboni-Okassa, J.-F. Fouquenet, S. Cohen-Jonathan, M. Soucé, H. Marchais, P. Dubois, *Analyst* **2005**, *130*, 1395.
58 Y.-S. Li, J. S. Church, A. L. Woodhead, *Journal of Magnetism and Magnetic Materials* **2012**, *324*, 1543.
59 C. Guo, Y. Hu, H. Qian, J. Ning, S. Xu, *Materials Characterization* **2011**, *62*, 148.
60 O. N. Shebanova, P. Lazor, *Journal of Raman Spectroscopy* **2003**, *34*, 845.
61 A. M. Jubb, H. C. Allen, *ACS Applied Materials & Interfaces* **2010**, *2*, 2804.
62 R. B. Kamble, V. Varade, K. P. Ramesh, V. Prasad, *AIP Advances* **2015**, *5*, 017119.
63 D. Baba, Y. Seiko, T. Nakanishi, H. Zhang, A. Arakaki, T. Matsunaga, T. Osaka, *Colloids and Surfaces B: Biointerfaces* **2012**, *95*, 254.
64 Seon-Ah Y., Sungmoon C., Seon Mi J., and Junhua Y., Scientific Reports, **2018**, *8*, 185.
65 I. A. Flores-Urquizo, P. García-Casillas, C. Chapa-González, *Revista Mexicana de Ingenieria Biomedica* **2017**, *38*, 402.

Magnetic nanoparticles are widely studied for biomedical applications. Cells interact with the surface of nanoparticles. It is important to know whether the coating affects both structural and magnetic properties. In the study we found that indeed, changes in both size and magnetization occur. Controlling and understanding the phenomena that occur at nanoparticle-cell interfaces will allow the optimization of nanomedicine systems.

I. A. Flores Urquizo, T. C. Hernández García, S. Lugo Loredo, J. T. Elizalde Galindo, P. E. García Casillas, J. C. Stevens Barrón*, C. Chapa González*

Influence of aminosilane nanoparticle coating on structural, magnetic and cell viability properties